FISEVIER

Contents lists available at ScienceDirect

## International Journal of Solids and Structures

journal homepage: www.elsevier.com/locate/ijsolstr





# Compression-induced buckling of thin films bonded to viscous substrates: Uniform wrinkles vs localized ridges

Xianheng Guan<sup>a</sup>, Anantha P. Sarma<sup>b,1</sup>, Eashwaren Kakarla Hamesh<sup>b,1</sup>, Junyu Yang<sup>b</sup>, Nhung Nguyen<sup>b,e</sup>, Enrique Cerda<sup>d</sup>, Luka Pocivavsek<sup>c,e</sup>, Sachin S. Velankar<sup>a,b,\*</sup>

- <sup>a</sup> Department of Mechanical Engineering and Material Science, University of Pittsburgh, Pittsburgh, PA, United States
- <sup>b</sup> Department of Chemical Engineering, University of Pittsburgh, Pittsburgh, PA, United States
- <sup>c</sup> Department of Surgery, University of Pittsburgh, Pittsburgh, PA, United States
- <sup>d</sup> Department of Physics, University of Santiago, Chile
- e Department of Surgery, University of Chicago, Chicago IL, United States

## ARTICLE INFO

Keywords: Wrinkling Folding Ridge Buckling Thin films

#### ABSTRACT

We examine the buckling of a thin elastic film bonded to a much thicker viscous substrate undergoing compression at a fixed rate. Experiments show two distinct buckling modes. At high rate of compression or at large liquid thickness, the buckles take on the form of approximately-sinusoidal wrinkles. At low rate of compression or at small liquid thickness, the buckles are highly localized into tall ridges separated nearly flat regions. Ridge growth is accompanied by lateral motion of the film in the near-ridge region, and the liquid in that region undergoes severe shear flow. Such ridge formation is entirely distinct from other examples of curvature localization such as fold localization of films on liquids in static equilibrium or ridge formation of films bonded to hyperelastic substrates. We quantify how the two lengthscales that arise from the buckling process, the wrinkle amplitude and the interridge distance, depend on compression rate and liquid thickness. We show that wrinkles formed during compression can also transform into ridges under quiescent conditions which suggests that buckle localization reduces bending energy of the film. We speculate that ridge localization appears due to a competition between two effects: a buckle mode with a few well-spaced ridges offers a lower energy state than uniform wrinkles, but wrinkles can develop faster because they require the viscous fluid to move over shorter distances.

## 1. Introduction

When a thin elastic film floating on a liquid substrate in gravity is compressed uniaxially, it buckles to form uniform, roughly sinusoidal, wrinkles. Upon further compression, one of the wrinkles evolves to become a large amplitude fold whereas the remaining wrinkles diminish. This localization of curvature is called the wrinkle-to-fold transition (Pocivavsek et al., 2008; Diamant and Witten, 2011; Démery et al., 2014; Rivetti, 2013; Oshri et al., 2015; Jambon-Puillet et al., 2016). A similar transition appears when the center of a floating thin film experiences compressive hoop stress, e.g. because its center is lifted upwards. Radial wrinkles appear at small vertical displacements, which then transform into more sharply localized radial ridges as the vertical displacement increases (Holmes and Crosby, 2010; Paulsen et al., 2016; Paulsen et al., 2017). Crumples are yet another form of

localized buckles on elastic sheets bonded to a liquid (King et al., 2012; Timounay et al., 2020). Films bonded to soft elastic substrates also show buckle localization, forming tall ridges or deep furrows. The localization sometimes takes on the form of period-doubling behavior (Brau et al., 2011; Cao and Hutchinson, 2012; Brau et al., 2013; Takei et al., 2014; Ebata et al., 2012). An excellent review of the variety of buckling modes, including effects of delamination, have been provided by Wang and Zhao (Wang and Zhao, 2014).

All these situations of thin film buckling on compliant substrate share two common features. First, all these systems exhibit at least two distinct buckling modes: one where the curvature in the thin film is distributed more-or-less evenly over the entire film (wrinkles), and another where the film curvature is large at some locations and nearly-zero elsewhere (folds, ridges, crumples). Second, all these situations can be regarded as "energy-conserving" in the sense that the substrate deformation needed

 $<sup>^{\</sup>star}$  Corresponding author.

E-mail address: velankar@pitt.edu (S.S. Velankar).

<sup>&</sup>lt;sup>1</sup> These authors contributed equally to this research.

to accommodate the film buckling can be described in terms of a potential energy contribution to the total system energy. Minimization of the total system energy can then predict the details of the buckling mode, whether the buckles are in the form of uniformly distributed wrinkles, localized folds, ridges, or other more complex patterns (Paulsen et al., 2016; King et al., 2012; Cai et al., 2011; Davidovitch et al., 2011; Holmes et al., 2008; Huang et al., 2010).

Previously we showed that an entirely different situation – an elastic film bonded to a viscous substrate - also shows buckle localization (Chatterjee et al., 2015). The phenomenon can be shown in a simple experiment conducted manually (see video file ManualExpt.mp4 available as Electronic Supplementary Information (ESI)). Following Fig. 1A&B, a strip of elastic film rests on the surface of a viscous liquid, which is itself coated onto a rubber strip being held stretched. Releasing the rubber strip imposes compressive stress on the liquid, which in turn compresses the film, causing it to buckle. Remarkably, the buckles can take on two distinct forms: wrinkles spread uniformly over the entire surface (Fig. 1A and first portion of ManualExpt.mp4), or tall and sharply-localized ridges separated by regions with small buckle amplitude (Fig. 1D&E and latter portion of ManualExpt.mp4). The differences between the two film widths in Fig. 1 will be discussed later. Crucially, since the liquid is viscous, the buckling behavior is rate-dependent; releasing the film slowly does not induce buckles at all (Chatterjee et al., 2015). The mechanics of such ridge localization is the central concern of this paper.

It is crucial to emphasize that the physics of buckling of elastic films on viscous supports (Sridhar et al., 2001) is radically different from the situations discussed in the first paragraph of this paper. For a compressed film of thickness h floating on a dense inviscid liquid in gravity, the wavelength is predicted to be  $\lambda = 2\pi (B/\rho g)^{1/4}$  where  $B = \frac{Eh^3}{12(1-\mu^2)}$  is

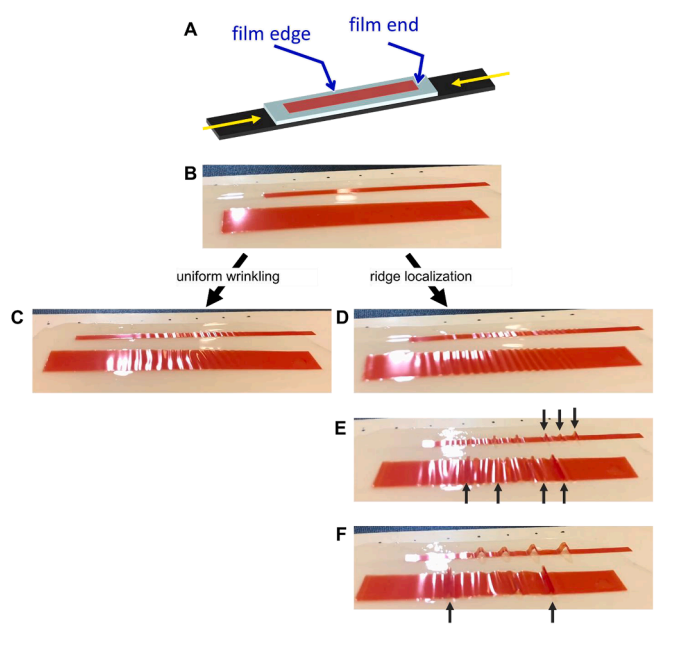


Fig. 1. A. Schematic of experiment corresponding to video ManualExpt.mp4. A film (orange) floats on a viscous liquid layer, which is itself placed on a prestretched rubber strip (black). The rubber strip is then allowed to relax (yellow arrows). B. Initial relaxed state where two films of different width are placed side-by-side to ensure that they have the same deformation. C. Uniform wrinkling regime. D-F. Ridge localization regime. Initial wrinkles transform into tall ridges, some of which are indicated by black arrows. For the narrower film, air rapidly enters under the narrow film making the ridges wider. Note that due to the high speed of the experiment and the hand-manipulation of the rubber, the frames are slightly blurred. (For interpretation of the references to colour in this figure legend, the reader is referred to the web version of this article.)

the bending stiffness of the film. Here E and  $\nu$  are the stiffness and Poisson ratio of the film, respectively. Using the parameter values film modulus E=5 *GPa*, film thickness h=0.025 *mm*,  $\nu=0.33$ , and liquid density  $\rho = 920 \text{ kg/m}^3$ ,  $\lambda = 33 \text{ mm}$  is estimated, which is at least one order of magnitude higher than the width of the ridges in Fig. 1B-E. This suggests that buckles in Fig. 1 do not result from a competition between film elasticity and gravity. Indeed our previous article showed that the buckling process was substantially similar even if the sample was tilted by 90° during compression, which suggests that gravitational effects are not a major factor in such buckling. Unlike ridges formed on elastic substrates which are in static equilibrium, the ridges seen here evolve and coarsen continuously with time, with some ridges growing and the others reducing in amplitude. In summary therefore, this buckling process cannot be regarded as a static equilibrium, and cannot be described as a competition between film bending energy vs gravity or vs surface tension or vs substrate elasticity. Indeed, viscous supports are not energy-conserving, but instead fully dissipate mechanical energy. Thus theoretical approaches based on energy conservation are not applicable; one must inherently account for the rate at which instabilities develop.

The first treatment of film wrinkling on viscous substrates as a kinetic process was conducted by Sridhar et al. (Sridhar et al., 2001) They showed that at any given value of compressive strain in the film, buckling is energetically-favored for wavelengths longer than a critical value. Viscosity serves to retard buckle growth, and more specifically, long wavelengths are retarded most severely because they require fluid motion over long distances. Thus the fastest-growing wavelength is a tradeoff between the magnitude of energy release due to wrinkling (longer wavelengths release more energy) and the kinetics of wrinkle growth (shorter wavelengths can grow faster). Since the original article detailing this insight, a series of articles of increasing complexity have refined the fundamental understanding of films on viscous supports (Chan et al., 2009; Chan et al., 2011; Chan et al., 2012; Sharp et al., 2006; Yin et al., 2003; Liang et al., 2002; Hobart et al., 2000; Huang and Suo, 2002; Huang and Suo, 2002; Huang, 2005; Im and Huang, 2005; Huang and Im, 2006; Yoo and Lee, 2003; Yoo and Lee, 2005; Yoo et al., 2004; Vandeparre and Damman, 2008; Vandeparre et al., 2010; Vandeparre et al., 2007; Mokni et al., 2008; Diamant, 2021; Chopin et al., 2017; Kodio et al., 2017).

Yet, none of the experimental, theoretical, or computational studies of wrinkling on viscous supports (Chan et al., 2009; Chan et al., 2011; Chan et al., 2012; Sharp et al., 2006; Yin et al., 2003; Liang et al., 2002; Hobart et al., 2000; Huang and Suo, 2002; Huang and Suo, 2002; Huang, 2005; Im and Huang, 2005; Huang and Im, 2006; Yoo and Lee, 2003; Yoo and Lee, 2005; Yoo et al., 2004; Vandeparre and Damman, 2008; Vandeparre et al., 2010; Vandeparre et al., 2007), mention buckle localization. In contrast, several examples of ridge formation have been reported in fully-elastic systems (Zang et al., 2012; Cao et al., 2014; Cao and Hutchinson, 2012; Zhao et al., 2015). An AFM image from Yoo et al (Yoo et al., 2004) of a buckled metal film on a viscoelastic polymer layer shows some flat regions separating tall buckles, yet, that article did not mention buckle localization. Kim et al (Kim et al., 2011) examined expansion of elastic films bonded to a partially-cured viscoelastic substrate. They reported that if the film modulus far exceeds the substrate modulus, tall ridges separated by flat regions appear. While Kim et al treated their substrate as a soft viscoelastic solid, it may share some of the same features as Fig. 1. However, it is not clear from these previous articles whether buckle localization is explained by the remaining elastic behavior of the substrate or can be explained in terms of purely viscous forces. At present even the most basic questions of buckle localization on viscous substrates remain unsettled, e.g. whether localization occurs at all liquid thicknesses, whether it is rate-dependent, whether ridges necessarily initiate at the edge of the film, and whether they have a preferred spacing. The goal of this article is to quantify this fascinating phenomenon experimentally to help guide further theoretical development. The observations here will also prove useful to develop textured surfaces for practical applications. For example, tall pillars or ridges are a common motif for surfaces with superhydrophobicity or adhesion (King et al., 2012; Timounay et al., 2020; Brau et al., 2011; Cao and Hutchinson, 2012; Brau et al., 2013; Takei et al., 2014; Ebata et al., 2012), and the aspect ratios produced using viscous supports are far higher than those on elastic substrates.

It is crucial to note the importance of using a prestretched rubber layer to compress the film (Fig. 1). Fundamental studies of buckle localization require compressing the film homogeneously. On liquid substrates, a floating film can be compressed homogeneously by pushing together the film ends (Pocivavsek et al., 2008; Jambon-Puillet et al., 2016; Huang et al., 2010; Wagner and Vella, 2011), analogous to a Langmuir trough. This method was used by Pocivavsek et al to study buckle localization at static equilibrium on inviscid substrates (Pocivavsek et al., 2008). But on viscous substrates, or indeed on any substrates that resist shear, that method cannot compress a long film homogeneously; the compression becomes confined to the regions near the film ends. Other methods such as pre-strain or a strain mismatch due to solvent swelling or differential thermal expansion can apply compression uniformly (Hobart et al., 2000; Yoo and Lee, 2003; Vandeparre and Damman, 2008), but do not allow control of the rate of deformation, which is crucial for viscous substrates. Nor do they permit large compressive strains, which (as this paper shows) favor ridge localization. The method used here and previously (Chatterjee et al., 2015), of using a prestretched rubber layer to compress the liquid, offers all three advantages: homogeneous compression of a long film, large strain ∈, and control of the strain rate ∈. This issue is discussed more thoroughly in ESI Section S1.

Early during this research, several crude experiments were conducted, and they show that the buckling process can be complex (Guan, 2022). Some of the complexity is illustrated by the difference in behavior of the two different widths in Fig. 1D-F. At short times during or after compression, both widths behave similarly and show the formation of tall ridges (Fig. 1E). However for the narrow film, the liquid layer rapidly recedes inwards under the peaks of the buckles allowing air to invade under the ridges, and thus allowing sharp ridges to become wider (Fig. 1F). The same happens for the wider film, but takes a longer time. Guided by those early observations (Guan, 2022), we conducted the experiments in this paper using a suitable film width so that the time for the air to invade the substrate far exceeds any other time in the experiment.

The layout of this paper is as follows. Section 2 describes the experimental procedure, and Section 3 describes the results of how strain rate and liquid layer thickness affects the buckling process, and quantify wavelength and interridge. We briefly discuss the results in Section 4, and conclude the paper in Section 5.

## 2. Experimental

While the basic phenomena of wrinkling and ridge localization can be illustrated easily by "hand" experiments such as Fig. 1, controlled experiments required careful selection of materials and geometry. Our previous article (Chatterjee et al., 2015) mentioned ridge formation only qualitatively; all the quantitative experiments examined wrinkle formation only. Guided by previous theory and numerical results (Guan et al., 2022), the experiments in this paper were designed specifically to examine ridge formation. Briefly, since the ends of the film are free, the film can relax the applied strain by end-relaxation (Chatterjee et al., 2015; Liang et al., 2002). Accordingly, there is always a buckle-free zone near the film ends. Sufficiently short films do not buckle at all, i.e. the buckle-free zone encompasses the entire film length. As film length increases, buckles develop, but they appear non-uniformly across the length of the film, as shown experimentally (Chatterjee et al., 2015) and also in simulations (Guan, 2022; Guan et al., 2022). The reason for the non-uniformity is that due to rapid end-relaxation, the film already develops a spatially-inhomogeneous strain state prior to buckling

(Chatterjee et al., 2015; Guan et al., 2022). In such situations, it is difficult to judge whether there is buckle localization or not since the number of buckles is relatively small. In contrast, for sufficiently long films, buckling across a long region near the center is nearly independent of end-relaxation. All the experiments in this paper were conducted with sufficiently long film length that end-relaxation can be ignored.

Materials: Butyl rubber strips of 1.58 mm thickness were cut to a width of either 1 in. (25.4 mm) or 0.5 in. (12.7 mm). The liquid used was BASF Oppanol B15, which is polyisobutylene (PIB) of molecular weight of roughly 85 kg/mol as quoted by the manufacturer. The rheological characteristics of this fluid are shown in ESI Fig. S1. The complex viscosity at low frequency is roughly 10<sup>6</sup> Pa.s, with modest shear thinning. In most of the experiments, the rates applied were on the order of 0.01 s<sup>-1</sup> and shear thinning effects, although present, may be modest. The highest rates in our experiments were roughly 0.09 s<sup>-1</sup> and shear thinning may be somewhat significant for these experiments. The fluid is also viscoelastic as judged by the significant magnitude of the storage modulus G' as compared to the loss modulus G''. At the conditions typical of most of the experiments (rates on the order of 0.01 s<sup>-1</sup> and strains of  $\sim 10\%$ ), we may estimate the stress contributions as follows: The fluid stresses attributable to viscous forces are on the order of (viscosity)  $\times$  (rate)  $\sim 10^6 \times~0.01 \sim 10^4$  Pa. The stresses attributable to elastic forces are on the order of (modulus)  $\times$  (strain)  $\sim 10^4 \, \times$  $0.1 \sim 1000 \ Pa$ . The fact that viscous stresses are 10-fold larger than elastic stresses suggests that most of the phenomena are due to viscosity, and hence a purely viscous Newtonian fluid would show the same phenomena, at least qualitatively. Indeed crude experiments (such as Fig. 1) conducted with an approximately Newtonian fluid show all the qualitative features noted in the careful experiments with Oppanol B15 PIB. Further, as will be shown in this paper, ridges appear at low rates, not high. This gives further confidence that the central interest of this paper – localization of buckles – is primarily a Newtonian fluid effect.

The films used in the experiments were polyester shimstock film purchased from McMaster-Carr Supply Co. with a film thickness of h=0.0254 mm. All experiments used a width of 8 mm.

<u>Sample preparation:</u> A long worm-like cylinder of polyisobutylene of the desired mass and length ( $\sim$ 130 mm) was placed lengthwise on the rubber strip. The PIB was then covered with a sheet of silicone rubber, pressed in a compression molding machine with the desired spacers to regulate the final compressed thickness, and silicone rubber layer removed.

The experimental setup illustrated in Fig. 2 consists of two cylindrical drums of diameter 44 mm which can be rotated by stepper motors. The rubber strip, already covered with the liquid layer, was clamped onto the surface of the drums. The drums were then counter-rotated to stretch the rubber strip. After waiting for several minutes to allow relaxation of any stresses in the liquid layer, the film of length 2L=100 mm was applied on the liquid surface. The film was then marked with highly diluted paint, either by spraying droplets, or bringing a paint-soaked thread lightly into contact with the surface. The drums were then counter-rotated at the desired circumferential velocity (denoted the *clamp velocity*) to allow the rubber strip to recover to the desired extent (roughly 15% strain). The central portion of the rubber strip rests on a lubricated flat surface which was raised a few mm with respect to the drums. This forces the rubber strip to remain flat, i.e. avoid tension-buckling along its width direction.

Imaging and image analysis: The experiment was video-recorded with a camera mounted at a shallow angle (Fig. 2). The actual strain rate experienced by the rubber strip was measured by digital image correlation analysis. The camera-facing edge of the rubber strip was marked with ink spots, and the Blender software was used to extract the displacement of these spots with time. The slope of these data gives the instantaneous strain. The procedure was described in detail previously (Chatterjee et al., 2015; Guan et al., 2022).

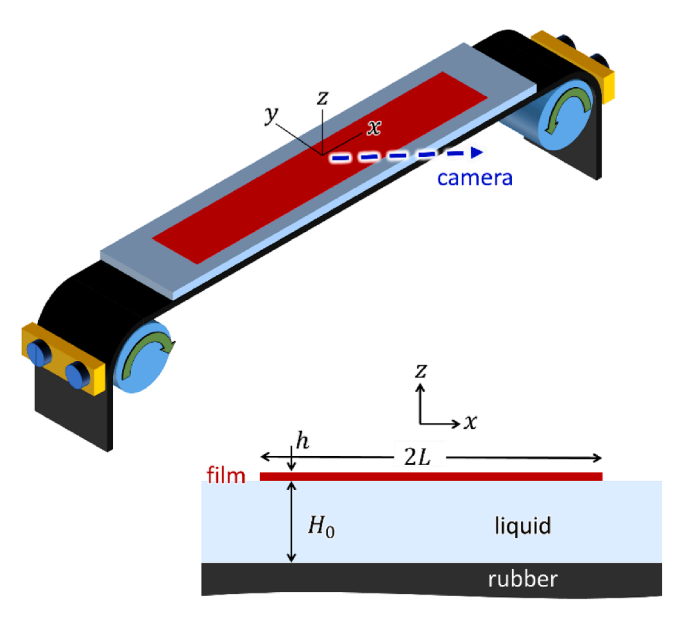


**Fig. 2.** Schematic of the experiment. Bottom right: cross-sectional view defining the geometric parameters. This schematic is not to scale; in fact 2L is far larger than h and  $H_0$ .

#### 3. Results

## 3.1. Qualitative aspects of uniform wrinkling vs ridge localization

Experiments were conducted at clamp velocities ranging from 0.1 to 10 mm/s, at liquid layer thicknesses  $H_0$  ranging from 0.25 mm to 1.59 mm. Several examples of the buckling process are shown in the video file Compression.mp4 available as ESI. The immediate qualitative conclusion from these videos is that low compression rates and small liquid

layer thicknesses both promote ridge localization, whereas high compression rates and large liquid thicknesses promote uniform wrinkling. This section uses frames from these videos to discuss some qualitative aspects of wrinkling and ridge localization.

To illustrate the extreme situations of wrinkling and ridge localization, Fig. 3 shows a sequence of frames extracted from two selected videos. Fig. 3A exemplifies the wrinkling situation which is more common at relatively large liquid layer thickness and rate. Upon being compressed from a flat state, at a strain of roughly 0.02, buckles with a few-mm wavelength appear across the entire film surface and grow steadily up to the end of the compression. In some experiments (see video), more complex phenomena may appear, e.g. coalescence of two neighboring peaks into a single one. Nevertheless, at the end of the compression process, the film has more-or-less uniform buckles everywhere.

Fig. 3B, exemplifies the situation of ridge localization which is more common at relatively small liquid layer thickness and rate. Even at the earliest stage when buckles first appear, they are not uniform across the surface; instead they appear in "packets" of relatively large amplitude, separated by regions with much smaller amplitude. Other examples of such packets are seen in the video Compression.mp4. With increasing strain, a few buckles grow much more than the others, whereas some of the surrounding buckles grow much less, or even reduce in amplitude. Occasional delaminations (Fig. 3B), presumably due to some defect at the liquid-film interface, do not appear to interfere with the evolution of neighboring buckles. By the end of the compression process, the film has tall buckles separated by regions that are more-or-less flat.

Experiments across the range of  $H_0$  and rate values show that this localized packet-like emergence of buckles becomes more pronounced as  $H_0$  or rate reduces. Indeed at the lowest rate and thickness examined (first experiment in the ESI video Compression.mp4, corresponding to  $H_0=0.25\ mm$ , rate of 0.0064  $s^{-1}$ ), ridges appear with barely perceptible neighboring wrinkles.

Close examination of the videos reveals a striking difference between

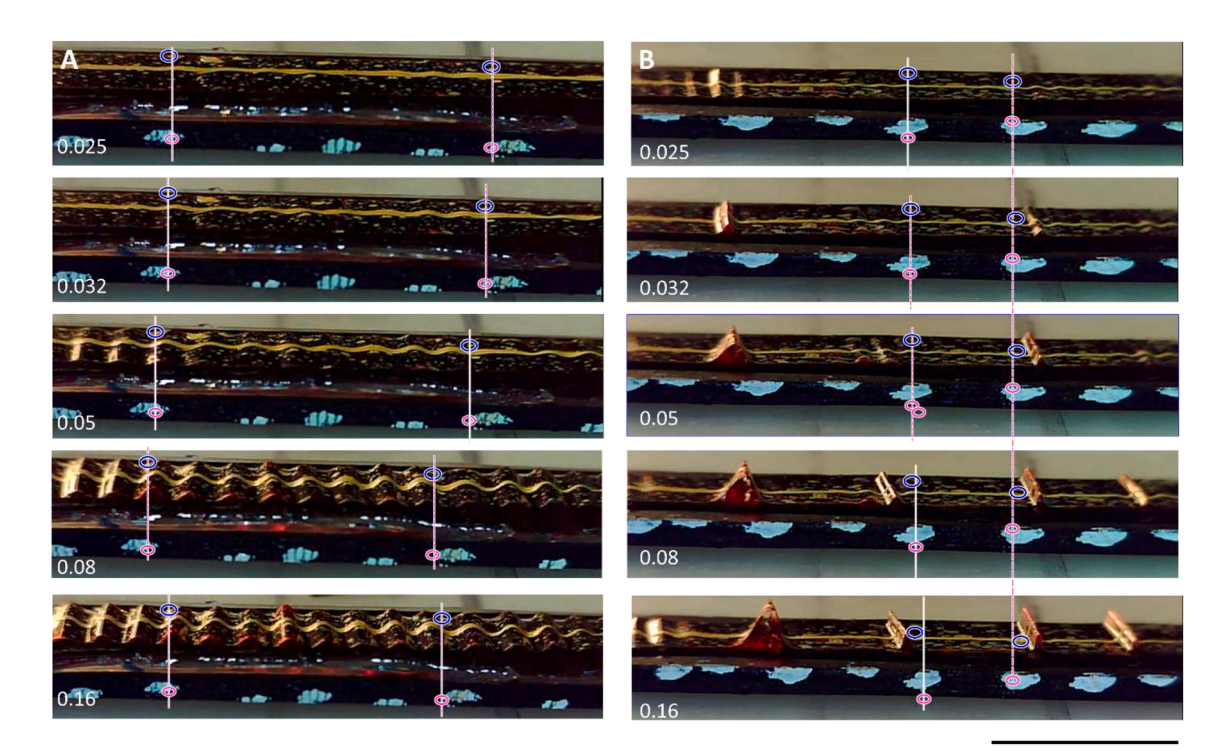


**Fig. 3.** Wrinkles (left) or localized ridges (right) developing under continuous compression. **A.**  $H_0 = 1.5$  mm,  $\dot{\epsilon} = 0.064$   $s^{-1}$ , corresponding to a clamp velocity of 10 mm/s for each clamp. **B.**  $H_0 = 0.25$  mm,  $\dot{\epsilon} = 0.019$   $s^{-1}$ , corresponding to a clamp velocity of 3 mm/s for each clamp. Film thickness is h = 0.025 mm in both cases. The black line on the bottom right is 10 mm. The numbers in each image correspond to the strain  $\epsilon$  in the rubber. The small arrows highlight complementary markers in the film and in the rubber layer.

wrinkling and ridge localization regimes, viz. in the ridge situation, the paint markers on the film undergo significant horizontal motion with respect to the rubber strip. To illustrate this, Fig. 3 compares markers on the film and on the rubber strip that are at the same horizontal position initially. The small pink ovals denote some well-defined small features on the rubber strip, and the dashed vertical pink lines are centered on these pink ovals. The blue ovals denote well-defined paint markers on the film surface. These are selected to be precisely above the pink markers in the top images. In Fig. 3A, the blue and pink markers remain approximately coincident along the horizontal direction throughout the experiment, i.e. material points on the film and material points in the rubber strip do not separate significantly along the x-direction. In Fig. 3B however, there is significant relative motion: material points on the film near the ridge "slide" horizontally towards the ridge over distances that appear to be far larger than  $H_0$ . Such sliding requires shear flow in the film and will be discussed further later.

While this paper is only focused on buckling behavior during compression, the films can also undergo significant changes under quiescent conditions as illustrated in Fig. 4, and the corresponding video QuiescentBehavior.mp4. This film was compressed under conditions corresponding to weak localization, and then compression was stopped. Accordingly, the initial state is almost homogeneously wrinkled, although some peaks are narrower and taller than others. However within 20 s after stopping compression, some of the wrinkles flattened significantly whereas others grew into localized ridges. This evolution continued so that at 180 s, tall ridges well-separated by much flatter regions are clearly evident. Yet, ridge localization is not an irreversible process. For example, the small red arrows mark two ridges that first grew and then reduced in amplitude. In contrast, the small blue arrows mark a ridge that grew monotonically. Thus Fig. 4 not only shows that wrinkles can change into localized ridges, but further that these films prefer an ever-increasing degree of localization, and hence any particular ridge may eventually lose amplitude to a neighboring ridge. A

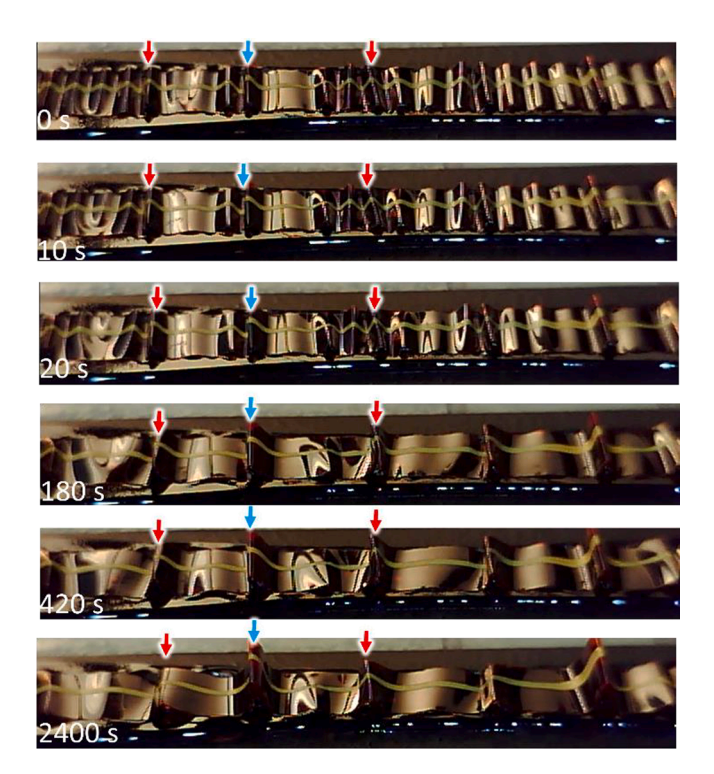


**Fig. 4.** Evolution of buckles under quiescent conditions after compression is stopped after a strain of 0.16. The top image corresponds to a nearly-homogeneous state of a sample with  $H_0 = 0.8 \ mm$  created by compressing at  $\dot{\epsilon} = 0.064 \ s^{-1}$ , corresponding to each clamp moving at 10 mm/s. The numbers correspond to the time in seconds after the end of compression.

separate experiment (see Fig. S3) confirms that gravitational effects are negligible during this quiescent evolution of buckles.

## 3.2. Wavelength and interridge distance

The videos show that at least two length scales emerge out of the buckling process: the wavelength,  $\lambda$ , and the interridge distance,  $\ell$ . These are plotted as a function of rate at fixed liquid thickness ( $H_0=0.25~mm$  in Fig. 5A) and as a function of liquid thickness at fixed rate ( $\dot{\epsilon}=0.064~s^{-1}$  in Fig. 5B). The dashed lines are power laws drawn only to guide the eye and give an approximate idea of sensitivity of  $\ell$  and  $\lambda$  to the liquid thickness and rate. We do not necessarily imply that a power law can represent these data over the entire range. The procedure for quantifying these distances from the videos is as follows.

Wavelengths can be estimated reliably by simply averaging the distance between neighboring peaks at a strain slightly past the critical value. These wavelengths, in the normalized form  $\lambda/H_0$ , are shown as filled red circles in Fig. 5A (for  $H_0=0.25$  mm). Note that Fig. 5A does not show a wavelength at the lowest rate because the film transitioned from a flat state to a ridged state with barely-perceptible wrinkles. Incidentally, while we quantify  $\lambda$  slightly after the onset of buckling, there is a small (less than 5% percent) decrease in wavelength as strain increases, but that magnitude is smaller than the error bars in Fig. 5.

Turning to interridge distances, for thin liquid layers, ridges are well-defined and hence  $\ell$  values can be estimated readily. Accordingly, Fig. 5A shows the normalized interridge distance  $\ell/H_0$  measured at a strain of 0.16, for  $H_0=0.25$  mm. In this figure, each blue  $\times$  corresponds one single  $\ell/H_0$  value in the experiment, and the blue diamonds are the arithmetic mean of these distances. Note that at the lowest rate in Fig. 5A, only three ridges are visible due to the large interridge distance, and hence only two interridge distances were measured.

For relatively thick liquid layers, e.g. some of the experiments of Fig. 5B, it is more difficult to quantify ℓ because the amplitude of the tallest buckles is not much larger than that of the other buckles. Thus it is no longer clear which buckles are "tall enough" to be classified as localized ridges. Especially challenging are cases when two tall buckles appear very close or adjacent to each other creating uncertainties about whether they are two separate localizations or not. For such situations, we exploited the fact that it is much easier to identify localized ridges immediately after the end of the compression, rather than during compression. This is clearly evident in Fig. 4 where, within 20 s after stopping compression, significant regions of the film rapidly become flat, allowing the localized ridges to be identified readily. Accordingly, for thicker liquid layers, inter ridge distances were measured from images taken about 30 s after compression was stopped. Such measurements are indicated by + symbols in Fig. 5B. This time is sufficiently short that there is no significant coalescence of neighboring ridges and the interridge distance thus-obtained is not sensitive to this delay time. Only after much longer times is there significant reorganization of ridges such as seen in Fig. 4.

A limited number of experiments also examined the rate-dependence at larger thicknesses, and those results are shown in Fig. S2. Once again note that at large thickness or large rate, ridges are difficult to identify and for those cases, interridge distances are not shown.

These quantifications of Fig. 5A and S2 support the following conclusions. First, the wavelength  $\lambda$  depends only weakly on rate (i.e.  $\lambda/H_0$  has a weak rate-dependence at fixed  $H_0$ ), and increases slightly as  $H_0$  increases (i.e.  $\lambda/H_0$  decreases less than  $H_0^{-1}$  at fixed rate). Second, with increasing rate,  $\ell$  decreases more than  $\lambda$ , whereas with increasing  $H_0$ ,  $\ell$  has roughly the same dependence as  $\lambda$ . Nevertheless we emphasize that in samples which show ridges,  $\ell$  is always several times of  $\lambda$ . The transition from ridged to wrinkled regimes with increasing rate or  $H_0$  occurs not because  $\ell$  approaches  $\lambda$ , but instead because the amplitude of the tallest ridges no longer dominates over all the others.

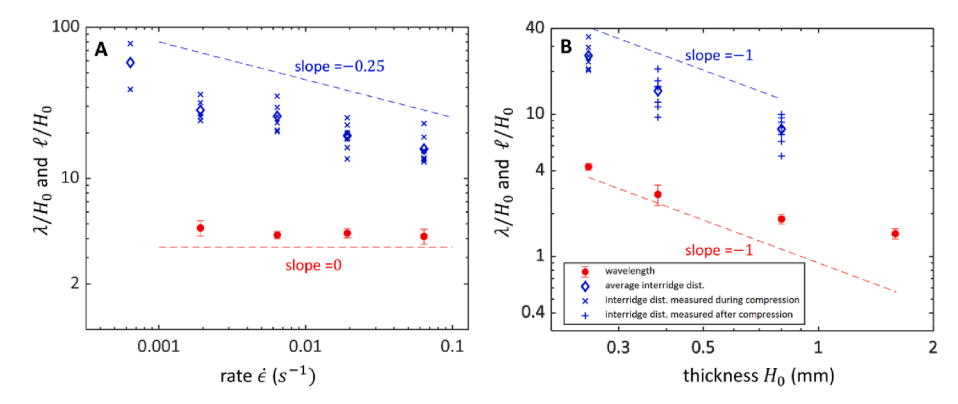


Fig. 5. Dependence of wavelength  $\lambda$  and interridge distance  $\ell$  (both normalized by liquid thickness  $H_0$ ) on **A**. compression rate at fixed  $H_0 = 0.25mm$  and **B**. liquid layer thickness at fixed rate  $\dot{\epsilon} = 0.064s^{-1}$ . Note that both axes are logarithmic in both plots.

## 3.3. Displacements of material points

We now turn to a more localized view of the buckling process, focusing not on averages, but on narrow regions that span only a few buckles. Although our video imaging was optimized for viewing relatively large areas of film to quantify interridge distances, the camera

resolution permits approximate quantification on the scale of individual buckles. This is done by tracking markers on the film surface, thus allowing measurements of buckle amplitudes as well as the horizontal displacements mentioned in Section 3.1.

Fig. 6 performs this quantification for two experiments corresponding respectively to wrinkling (left column of Fig. 6) and ridge

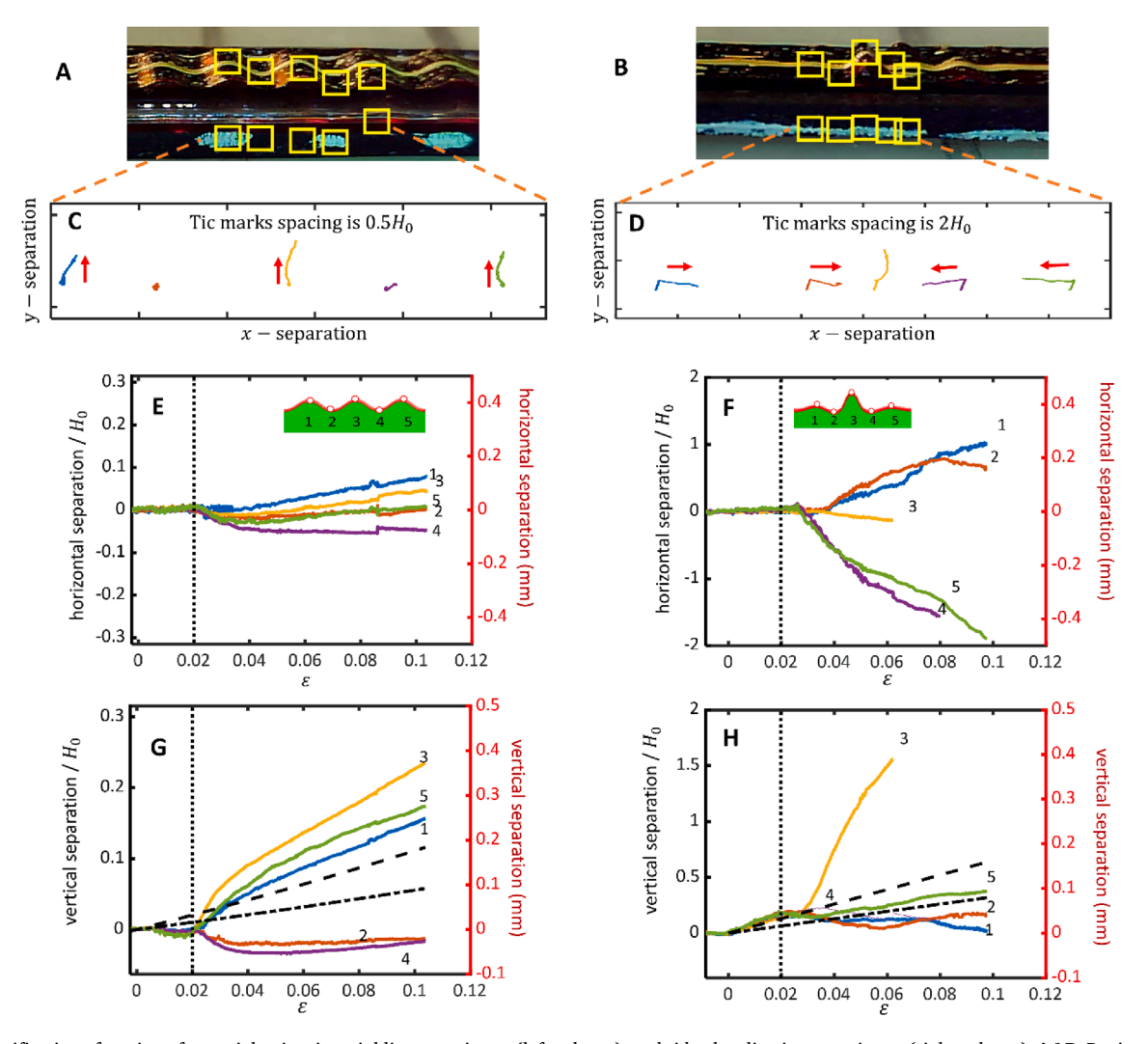


Fig. 6. Quantification of motion of material points in wrinkling experiment (left column), and ridge localization experiment (right column). A&B: Regions of interest selected for estimating displacements. The yellow boxes indicate the material locations that are tracked. C&D: Spatial trajectories of marker separations (see text). E&F: Horizontal separation (see text for definition) vs strain, and G&H: Vertical separation vs strain. Dotted vertical lines in E-H are the strains at which buckles were first visible in the video. (For interpretation of the references to colour in this figure legend, the reader is referred to the web version of this article.)

localization (right column of Fig. 6). For this quantification, we track pairs of markers: one ink marker on the film and an immediately-adjacent ink mark along the edge of the rubber (see Fig. 6A and B). The difference between the displacements of a marker on the film and the corresponding marker on the rubber, dubbed *separation* in the rest of this section, approximates the relative motion of material points in the film relative to underlying material points in the rubber substrate. Note in the absence of buckling, vertical separation between a pair of markers would increase due to the incompressibility of the rubber and of the liquid layer. Fig. 6C and D plots the spatial-trajectories of the separation for five pairs of markers. These same trajectories are shown as a function of strain in Fig. 6E-H. In these plots, the actual separations can be read off the right y-axes, and the separation normalized by  $H_0$  on the left y-axes.

Fig. 6A corresponds to the development of a roughly homogeneous wrinkled state, and we track five markers which eventually become three adjacent peaks and two intermediate troughs in the homogeneously-wrinkled region. The spatial trajectories (Fig. 6C) show approximately vertical motion of the peaks, whereas the troughs show little displacement. When examined as a function of strain, the vertical separation of the markers (Fig. 6G) shows behavior typical of a wrinkling transition wherein all markers move in tandem up to buckling, followed by a sharp increase in the separation of the peak markers and a decrease in the separation of the trough markers. Further, over most of the experimental time, the horizontal separation of the markers (Fig. 6E) remains small with no sharp changes with strain.

Fig. 6B corresponds to ridge formation, and once again, five markers are tracked: one corresponding to the peak of a ridge, two corresponding to neighboring peaks, and two corresponding to the intermediate troughs. Fig. 6D shows a sharp difference with respect to Fig. 6C: the peak of the ridge moves almost vertically, whereas the neighboring markers have predominantly horizontal motion. Examining the strain dependence, at small strain, all five markers move in concert, with the horizontal separation remaining near zero. At a strain of roughly 0.03, the vertical separation of the central marker starts increasing rapidly while the others no longer increase (Fig. 6H). Simultaneously, all the markers start moving inwards towards the central marker (Fig. 6F).

The differences between wrinkling and ridge localization are much more stark when recast in non-dimensional terms, which corresponds to the left y-axes in Fig. 6E-H. The non-dimensional amplitude of the ridge is almost 4-times larger than of the wrinkles. Further, the ratio of the horizontal separation to  $H_0$  is a measure of the local shear strain in the fluid, and a comparison of Fig. 6E vs G shows that this shear strain is at least an order of magnitude larger in the ridge situation. Further, the markers near the central peak in Fig. 6F show a shear strain of as much as 1.5 strain units, which is 10-fold larger than the applied compressive strain. By implication, the shear rate in the liquid is also 10-fold larger than the applied compression rate.

## 4. Discussion

To summarize the three central experimental observations, (1) tall ridges separated by mostly-flat regions appear at low rates and low liquid thicknesses; (2) with increasing rate or liquid thickness, the differences between the amplitude of tallest buckles vs the others buckles diminish until the samples are deemed to be uniformly buckled; and (3) ridge growth (but not wrinkling) is accompanied by significant horizontal motion of the film.

We now speculate on the mechanics of ridge localization. Section 3.1 noted that even samples that show uniform wrinkles during compression evolve into localized ridges after the compression is stopped. This suggests that localized ridges provide a lower energy state than uniformly-distributed wrinkles. Yet, the fact that ridges only appear upon slow compression suggests that ridges are kinetically limited, presumably because development of well-spaced ridges requires displacing the film (and the underlying fluid) over relatively large distances. This is not due

to any unique characteristics of ridges, but common to *any* instability in which viscosity plays a retarding role, e.g. capillary instabilities of viscous threads (Tomotika, 1935), spinodal decomposition in the bulk (Haskell, 1973), spinodal dewetting of thin films (Vrij, 1966), buckling of elastic fibers in viscous media (Jiang and Zhang, 2008), or indeed sinusoidal wrinkling of elastic films on viscous supports (Sridhar et al., 2001; Huang and Suo, 2002). In all these cases, long-wavelength instabilities are energetically-favorable, but penalized by their slow kinetics. We therefore propose that uniform wrinkling appears at high compression rate because it only requires fluid motion over short distances (a single wavelength). In contrast, at low compression rate, the film has adequate time to also move over distances much larger than the wavelength, and therefore ridges can develop.

The effect of the liquid layer can be thought of in three distinct ways: gravity, incompressibility and viscosity. The first effect of the liquid, that it induces a gravitational penalty for any variation in film height, is relevant in many static loading situations. This effect is ignored here since gravitational effects are negligible at least over the timescale of the loading process. In fact we had confirmed previously (Chatterjee et al., 2015) that tilting the sample by  $90^{\circ}$  made no qualitative difference to ridge formation.

The second effect is relevant to sufficiently wide films for which exchange of fluid across the side edge of the film (see Fig. 1A) is negligible over the timescale of the compression. Accordingly the fluid imposes an incompressibility constraint so that the volume of fluid under the buckles must be preserved. This liquid incompressibility condition clearly shows why a localized buckle is energetically-favorable. Specifically, consider the following 2D problem posed in purely geometric terms: An elastica of length 2L is placed parallel to an underlying flat surface at a certain distance  $H_0 \ll 2L$  as illustrated in Fig. 7A. The end-toend distance of the elastica is now reduced by  $\Delta = 2L \in$  so that the elastica must be accommodated within the length  $2L(1-\epsilon)$ , while maintaining its contour length. Crucially, fluid incompressibility forces the area between the elastica and the underlying flat surface to remain at a value of  $2LH_0$ . At small values of strain  $\in$ , the two constraints (length of elastica and area under the elastica) can be satisfied by a single sinusoidal profile (Fig. 7B-a) with a wavelength spanning the system length. At small strain, the amplitude of this single sinusoid, which can be calculated by setting its contour length to 2L, is proportional to  $L\sqrt{\epsilon}$ (Vandeparre et al., 2011). With increasing strain, the amplitude increases until the film is forced to contact the underlying surface. It seems intuitive that in such a situation, the lowest energy state is not multiple buckles, but a single localized buckle of a shape qualitatively illustrated in Fig. 7B-b. But realizing such a shape requires fluid motion over distances comparable to the entire film. For sufficiently long films, the timescale associated with such fluid motion must far exceed the timescale  $\dot{\epsilon}^{-1}$  over which compression is applied. Thus, multiple buckles (ridges or wrinkles) appear at finite rate of compression because they allow the elastic energy to decrease as compared to the flat state, albeit not to the minimum value of Fig. 7B-b.

An unexpected result from our experiments (see video Compression. mp4) is that buckles first appear in "packets", which then grow into ridges with no change in position. We conjecture that these packets of wrinkles add natural imperfections to the film and select the positions where ridges may develop. These packets are a sign of the large length scale modulation of the horizontal motion which is necessary to reduce elastic energy of the film while being compatible with dissipation in the fluid. The imperfections develop into ridges only if their amplitude can grow sufficiently rapidly as compared to the primary wrinkles. We therefore propose Fig. 7C as the mechanism whereby buckles grow as localized ridges or uniform wrinkles when compression is applied at a finite rate. Due to the packets at the buckle threshold (Fig. 7C-a), some regions have higher amplitude than others. Since buckling relieves compressive strain, these high-amplitude regions have lower film strain than their neighboring regions. The resulting film strain gradient

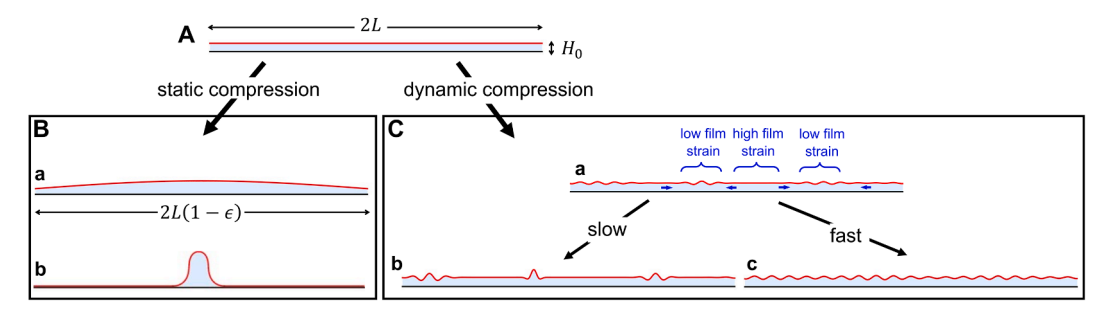


**Fig. 7. A.** Schematic of an elastica (red) placed at a distance  $H_0$  from a surface (rubber layer) shown in black. **Box B.** Shapes expected if the elastica minimizes energy at small strain (**B-a**) and large strain (**B-b**). **Box C.** Compression at finite rate. **C-a.** Packets of buckles appear at small strain. Regions with high amplitude have lower film strain, and the corresponding strain gradient induces horizontal film motion (blue arrows). **C-b.** This causes the growth of localized ridges if compression is slow. **C-c.** At high compression rate, additional buckles grow between the packets giving approximately-uniform wrinkles. (For interpretation of the references to colour in this figure legend, the reader is referred to the web version of this article.)

induces a stress in the film that pushes the film from the low-amplitude to high-amplitude region (Fig. 7C-a), thus making the ridges taller (Fig. 7C-b). Crucially, this horizontal motion also relieves the compressive strain in the adjacent film, thus inhibiting buckle growth in the region around the ridges. Indeed the same mechanism is active near the film ends: a gradient in film strain induces horizontal motion at the film ends (which can be captured by the shear lag model Chatterjee et al., 2015; Liang et al., 2002), thus suppressing buckling near the ends. In the present situation, since ridge growth requires film motion over multiple wavelengths, it is possible only at relatively low compression rates. At high compression rate, horizontal motion is too slow to relieve compression in the neighboring regions, and hence buckles grow everywhere (Fig. 7C-c) giving nearly uniform wrinkles. The driving force for localization persists however, and therefore after stopping compression, wrinkles gradually localize into ridges at the positions where natural imperfections are settled. Indeed, numerical simulations confirm that well-spaced buckles offer a lower energy than closelyspaced wrinkles (Guan, 2022; Guan et al., 2022).

In the above physical picture, horizontal motion of the film is crucial to

ridge growth, as was indeed shown in Fig. 3. This horizontal motion of the

film is regulated by the third effect of the fluid layer, which is to retard flow between the film and the rubber strip. It is helpful to think of the film motion parallel to the rubber strip separately from the motion perpendicular to the strip. For two parallel surfaces moving perpendicular to each other at a specified rate, lubrication theory (Leal, 2007) states that the viscous resistance scales as  $H^{-3}$  where H is the local liquid thickness. Accordingly, for sinusoidal wrinkles of amplitude 2A, the viscous resistance under the trough (  $[H_0-A]^{-3}$  ) may far exceed that under the peak  $([H_0 + A]^{-3})$ , thus causing a large up-down asymmetry between peaks and troughs. This asymmetry is such that the liquid thickness under a peak can change readily, whereas the liquid thickness under a trough cannot. This asymmetry by itself would not induce localization; it would only cause initially-sinusoidal wrinkles to develop increasingly flat troughs as the strain increases. Ridge growth further requires long-range film motion parallel to the rubber strip. As per lubrication theory, the viscous resistance to local parallel motion between the film and the rubber strip scales as  $H^{-1}$ , a dependence that is far less severe as compared to perpendicular motion. Thus, with the film strain gradient (previous paragraph) as the driving force, one ridge may grow rapidly by "gathering up" the contour length of neighboring ridges or wrinkles.

Although much of the literature in this area assumes that the film behaves inextensibility, our experiments show that extensibility plays a fundamental role to explain localization. Indeed, the time scale to reach the critical strain for buckling  $\epsilon_c$  should be  $\tau \sim \epsilon_c/\dot{\epsilon}$  which can be longer or shorter depending on the strain rate. An implicit assumption when using inextensibility is that this time scale is very short and more complex phenomena such as localization appear after for times longer than  $\tau$ ,

i.e. after buckling (Auguste et al., 2018; Brau et al., 2011). However, the results in this paper show that the selection of wrinkling or ridges for viscous substrates appear for times similar to  $\tau$  when the extensibility of the film is significant.

All the experiments in this paper use films that were long enough to approximate infinite length conditions. The discussion above presumes that end-effects are negligible. In fact, for finite length films, relaxation of the films from the ends competes with wrinkling and ridge formation. Just as lateral motion near a ridge relieves in-plane compression, so does lateral motion near the ends. Hence reducing film length while keeping other parameters fixed would suppress both wrinkling and ridge formation.

## 5. Conclusions

We have examined the buckling of a thin elastic film bonded to a thicker viscous layer undergoing compression at a fixed rate. The physics of such buckling is entirely different from the more well-studied examples of static buckling of elastic films floating on liquids or films attached to soft elastic supports. Those cases conserve mechanical energy, while the present situation is fully-dissipative due to the viscous nature of the liquid layer. Experiments were conducted by placing a narrow strip of film atop a wider viscous layer, which was itself bonded to a pre-stretched rubber strip. Unstretching the rubber strip induced uniaxial compression of the liquid, which then transferred the compression to the film. Crucially, this method allowed the film to experience uniform compression over almost its entire length, which would not be possible if the ends of the film were compressed directly. The viscous layer was nearly-Newtonian, 10-80 times thicker than the film, and sufficiently long that infinite-length conditions are approximated.

Our experiments make three central observations. (1) Two distinct buckling modes are possible. Thick liquid layers or fast compression rates induce approximately-sinusoidal wrinkles over the entire film. In contrast, thin liquid layers or slow compression rates induce highly localized tall ridges which are separated by regions that are nearly flat. (2) Upon cessation of compression, under quiescent conditions, the tallest buckles grow whereas the others diminish. This suggests that an increasing degree of buckle localization reduces bending energy. (3) Ridge formation is associated with large lateral motion of the film, and the liquid near the ridge undergoes a shear strain that is 10-fold larger than the applied compressive strain.

We propose the following underlying mechanism. The liquid imposes an incompressibility constraint wherein the volume under the buckled film is fixed. Under this constraint, the lowest energy state corresponds to a single tall ridge. However developing a single ridge requires moving the fluid over distances comparable to the film length. Since the fluid is viscous, this process can take a long time. Thus, well-separated ridges

appear as a temporary state which allows a lower energy than uniformly-distributed wrinkles.

The type of ridge formation described here is altogether different from the ridge formation seen for stiff films on prestretched hyperelastic substrates. It requires both, that the substrate be able to accommodate an arbitrarily large deformation (which permits well-separated ridges to appear) and that the substrate penalize fast motion (thus favoring ridges rather than wrinkles at low compression rate).

## **Declaration of Competing Interest**

The authors declare that they have no known competing financial interests or personal relationships that could have appeared to influence the work reported in this paper.

## Acknowledgements

This research was supported by NSF-1561789, NSF-1636064, NSF-1824708 and NIH R56-HL142743-01. EC acknowledges the support of Fondecyt Grant No 1201250. A.P.S. and E.K.H. are grateful to a travel grant from Sastra University, Thanjavur, India, which supported their research. We are grateful to Prof. Rui Huang, U. Texas for discussions.

## Appendix A. Supplementary data

Supplementary data to this article can be found online at https://doi. org/10.1016/j.ijsolstr.2022.111843.

## References

- Auguste, A., Yang, J., Jin, L., Chen, D., Suo, Z., Hayward, R.C., 2018. Formation of high aspect ratio wrinkles and ridges on elastic bilayers with small thickness contrast. Soft Matter 14, 8545-8551.
- Brau, F., Vandeparre, H., Sabbah, A., Poulard, C., Boudaoud, A., Damman, P., 2011. Multiple-length-scale elastic instability mimics parametric resonance of nonlinear oscillators. Nat. Phys. 7, 56-60.
- Brau, F., Damman, P., Diamant, H., Witten, T.A., 2013. Wrinkle to fold transition: influence of the substrate response. Soft Matter 9, 8177-8186.
- Cai, S., Breid, D., Crosby, A.J., Suo, Z., Hutchinson, J.W., 2011. Periodic patterns and energy states of buckled films on compliant substrates. J. Mech. Phys. Solids 59, 1094-1114.
- Cao, C., Chan, H.F., Zang, J., Leong, K.W., Zhao, X., 2014. Harnessing localized ridges for high-aspect-ratio hierarchical patterns with dynamic tunability and multifunctionality. Adv. Mater. 26, 1763-1770.
- Cao, Y., Hutchinson, J.W., 2012. From wrinkles to creases in elastomers: the instability and imperfection-sensitivity of wrinkling. Proceed. Roy. Soc. A: Mathemat., Phys. Eng. Sci. 468, 94-115.
- Cao, Y., Hutchinson, J.W., 2012. Wrinkling Phenomena in Neo-Hookean Film/Substrate Bilayers. J. Appl. Mech. 79, 031019.
- Chan, E.P., Page, K.A., Im, S.H., Patton, D.L., Huang, R., Stafford, C.M., 2009. Viscoelastic properties of confined polymer films measured via thermal wrinkling. Soft Matter 5, 4638-4641.
- Chan, E.P., Kundu, S., Lin, Q.H., Stafford, C.M., 2011. Quantifying the Stress Relaxation Modulus of Polymer Thin Films via Thermal Wrinkling. ACS Appl. Mater. Interfaces 3, 331-338.
- Chan, E.P., Lin, O., Stafford, C.M., 2012. Quantifying the elasticity and viscosity of geometrically confined polymer films via thermal wrinkling. J. Polym. Sci. Part B-Polym. Phys. 50, 1556–1561.
- Chatterjee, S., McDonald, C., Niu, J., Velankar, S.S., Wang, P., Huang, R., 2015. Wrinkling and folding of thin films by viscous stress. Soft Matter 11, 1814-1827.
- Chopin, J., Dasgupta, M., Kudrolli, A., 2017. Dynamic wrinkling and strengthening of an elastic filament in a viscous fluid. Phys. Rev. Lett. 119, 088001.
- Davidovitch, B., Schroll, R.D., Vella, D., Adda-Bedia, M., Cerda, E.A., 2011. Prototypical model for tensional wrinkling in thin sheets. PNAS 108, 18227–18232.
- Démery, V., Davidovitch, B., Santangelo, C.D., 2014. Mechanics of large folds in thin interfacial films. Phys. Rev. E 90, 042401.
- Diamant, H., 2021. Parametric excitation of wrinkles in elastic sheets on elastic and viscoelastic substrates. Soft Matter 44, 78.
- Diamant, H., Witten, T.A., 2011. Compression induced folding of a sheet: An integrable system. Phys. Rev. Lett. 107, 164302.
- Ebata, Y., Croll, A.B., Crosby, A.J., 2012. Wrinkling and strain localizations in polymer thin films. Soft Matter 9086-9091.
- Guan, X.; Pocivavsek, L.; Nguyen, N.; Cerda, E.; Velankar, S. S. Compression-induced buckling of thin films bonded to viscous substrates: Film Length effect (To be submitted). 2022.

- Guan, X.; Nguyen, N.; Cerda, E.; Pocivavsek, L.; Velankar, S. S. 2022. Dynamics of wrinkling, ridge localization, and end relaxation of thin films bonded to viscous substrates (submitted to Int. J. Solid. Struct.).
- Guan, X., Reddipalli, L., Butler, D., Liu, Q., Velankar, S.S., 2022. Rate-dependent creasing of a viscoelastic liquid. Extreme Mech. Lett. In press
- Guan, X. 2022. Compression rate-dependent buckling and creasing mechanics of elastic and viscoelastic films. University of Pittsburgh, Ph.D. thesis.
- Haskell, R.W., 1973. Introduction to thermodynamics of spinodal decomposition. J. Am. Ceram, Soc. 56, 355-360.
- Hobart, K.D., Kub, F.J., Fatemi, M., Twigg, M.E., Thompson, P.E., Kuan, T.S., Inoki, C.K., 2000. Compliant substrates: A comparative study of the relaxation mechanisms of strained films bonded to high and low viscosity oxides. J. Electron. Mater. 29,
- Holmes, D.P., Crosby, A.J., 2010. Draping Films: A Wrinkle to Fold Transition. Phys. Rev. Lett. 105, 038303
- Holmes, D.P., Ursiny, M., Crosby, A.J., 2008. Crumpled surface structures. Soft Matter 4,
- Huang, R., 2005. Kinetic wrinkling of an elastic film on a viscoelastic substrate. J. Mech. Phys. Solids 53, 63-89.
- Huang, J., Davidovitch, B., Santangelo, C.D., Russell, T.P., Menon, N., 2010. Smooth cascade of wrinkles at the edge of a floating elastic film. Phys. Rev. Lett. 105,
- Huang, R., Im, S.H., 2006. Dynamics of wrinkle growth and coarsening in stressed thin films. Phys. Rev. E - Statist., Nonlin. Soft Matt. Phys. 74, 026214.
- Huang, R., Suo, Z., 2002. Instability of a compressed elastic film on a viscous layer. Int. J. Solids Struct. 39, 1791-1802.
- Huang, R., Suo, Z., 2002. Wrinkling of a compressed elastic film on a viscous layer. J. Appl. Phys. 91, 1135–1142.
- Im, S.H., Huang, R., 2005. Evolution of wrinkles in elastic-viscoelastic bilayer thin films. J. Appl. Mechan.-Trans. Asme 72, 955-961.
- Jambon-Puillet, F., Vella, D., Protière, S., 2016. The compression of a heavy floating elastic film. Soft Matter 12, 9289-9296.
- Jiang, H.O., Zhang, J.P., 2008. Mechanics of Microtubule Buckling Supported by Cytoplasm. J. Appl. Mechan.-Trans. Asme 75, 061019.
- Kim, P., Abkarian, M., Stone, H.A., 2011. Hierarchical folding of elastic membranes under biaxial compressive stress. Nat. Mater. 10, 952–957.
- King, H., Schroll, R.D., Davidovitch, B., Menon, N., 2012, Elastic sheet on a liquid drop reveals wrinkling and crumpling as distinct symmetry-breaking instabilities. PNAS 109, 9716-9720.
- Kodio, O., Griffiths, I.M., Vella, D., 2017, Lubricated wrinkles: Imposed constraints affect the dynamics of wrinkle coarsening. Phys. Rev. Fluids 2, 014202.
- Leal, L.G., 2007. Chapter 5: The Thin-Gap Approximation Lubrication Problems. In Advanced Transport Phenomena: Cambridge University Press, Cambridge,
- Liang, J., Huang, R., Yin, H., Sturm, J.C., Hobart, K.D., Suo, Z., 2002. Relaxation of
- compressed elastic islands on a viscous layer. Acta Mater. 50, 2933–2944.

  Mokni, N., Kostrzewa, M., Sidoroff, F., 2008. Instability of an elastic film on a viscous layer, Europ. J. Mechan. A/Solids 27, 783-795.
- Oshri, O., Brau, F., Diamant, H., 2015. Wrinkles and folds in a fluid-supported sheet of finite size. Phys. Rev. E 91, 052408.
- Paulsen, J.D., Hohlfeld, E., King, H., Huang, J.S., Qiu, Z.L., Russell, T.P., Menon, N., Vella, D., Davidovitch, B., 2016. Curvature-induced stiffness and the spatial variation of wavelength in wrinkled sheets. PNAS 113, 1144-1149.
- Paulsen, J.D., Demery, V., Toga, K.B., Qiu, Z.L., Russell, T.P., Davidovitch, B., Menon, N., 2017. Geometry-Driven Folding of a Floating Annular Sheet. Phys. Rev. Lett. 118, 048004
- Pocivavsek, L., Dellsy, R., Kern, A., Johnson, S., Lin, B., Lee, K.Y.C., Cerda, E., 2008. Stress and fold localization in thin elastic membranes. Science 320, 912-916.
- Rivetti, M., 2013. Non-symmetric localized fold of a floating sheet. Comptes rendus mécanique 341, 333-338.
- Sharp, J.S., Vader, D., Forrest, J.A., Smith, M.I., Khomenko, M., Dalnoki-Veress, K., 2006. Spinodal wrinkling in thin-film poly(ethylene oxide)/polystyrene bilayers. Europ. Phys. J. E 19, 423-432.
- Sridhar, N., Srolovitz, D.J., Suo, Z., 2001. Kinetics of buckling of a compressed film on a viscous substrate. Appl. Phys. Lett. 78, 2482-2484.
- Takei, A., Jin, L., Hutchinson, J.W., Fujita, H., 2014. Ridge localizations and networks in thin films compressed by the incremental release of a large equi-biaxial pre-stretch in the substrate. Adv. Mater. 26, 4061-4067.
- Timounay, Y., De, R., Stelzel, J.L., Schrecengost, Z.S., Ripp, M.M., Paulsen, J.D., 2020. Crumples as a generic stress-focusing instability in confined sheets. Phys. Rev. X 10, 021008.
- Tomotika, S., 1935. On the instability of a cylindrical thread of a viscous liquid surrounded by another viscous fluid. In: Proceedings of the Royal Society of London, pp. 322-337.
- Vandeparre, H., Damman, P., 2008. Wrinkling of stimuloresponsive surfaces: Mechanical instability coupled to diffusion. Phys. Rev. Lett. 101, 124301.
- Vandeparre, H., Leopoldes, J., Poulard, C., Desprez, S., Derue, G., Gay, C., Damman, P., 2007. Slippery or sticky boundary conditions: Control of wrinkling in metal-capped thin polymer films by selective adhesion to substrates. Phys. Rev. Lett. 99, 188302.
- Vandeparre, H., Gabriele, S., Brau, F., Gay, C., Parker, K.K., Damman, P., 2010. Hierarchical wrinkling patterns. Soft Matter 6, 5751–5756.
- Vandeparre, H., Piñeirua, M., Brau, F., Roman, B., Bico, J., Gay, C., Bao, W., Lau, C.N., Reis, P.M., Damman, P., 2011. Wrinkling Hierarchy in Constrained Thin Sheets from Suspended Graphene to Curtains. Phys. Rev. Lett. 106, 224301.
- Vrij, A. 1966 Possible mechanism for spontaneous rupture of thin free liquid films. Discussions of the Faraday Society, 23-&...

- Wagner, T.J.W., Vella, D., 2011. Floating Carpets and the Delamination of Elastic Sheets. Phys. Rev. Lett. 107, 044301.
- Wang, Q., Zhao, X., 2014. Phase Diagrams of Instabilities in Compressed Film-Substrate Systems. J. Appl. Mechan. 81, 0510041–5100410.
- Yin, H.Z., Huang, R., Hobart, K.D., Liang, J., Suo, Z., Shieh, S.R., Duffy, T.S., Kub, F.J., Sturm, J.C., 2003. Buckling suppression of SiGe islands on compliant substrates. J. Appl. Phys. 94, 6875–6882.
- Yoo, P.J., Lee, H.H., 2003. Evolution of a stress-driven pattern in thin bilayer films: Spinodal wrinkling. Phys. Rev. Lett. 91, 154502.
- Yoo, P.J., Lee, H.H., 2005. Morphological diagram for metal/polymer bilayer wrinkling: Influence of thermomechanical properties of polymer layer. Macromolecules 38, 2820–2831.
- Yoo, P.J., Suh, K.Y., Kang, H., Lee, H.H., 2004. Polymer elasticity-driven wrinkling and coarsening in high temperature buckling of metal-capped polymer thin films. Phys. Rev. Lett. 93, 034301.
- Zang, J., Zhao, X., Cao, Y., Hutchinson, J.W., 2012. Localized ridge wrinkling of stiff films on compliant substrates. J. Mech. Phys. Solids 60, 1265–1279.
- Zhao, Y., Cao, Y., Hong, W., Wadee, M.K., Feng, X.-Q., 2015. Towards a quantitative understanding of period-doubling wrinkling patterns occurring in film/substrate bilayer systems. Proceed. Mathemat., Phys., Eng. Sci. 471, 20140695.